# Accelerating elastoplastic material models with spare nonlinear regression: A hybrid approach

G. Bokil[1], D. Koch[2], André Haufe[2], Holger Steeb[3]

[1,3]University of Stuttgart, Pfaffenwaldring, D-70569 Stuttgart
[2]DYNAmore GmbH, an ANSYS company, Industriestrasse 2, D-70565 Stuttgart

## 1 Abstract

Evaluating material models in Finite Element (FE) simulations is computationally expensive. Recently, Machine Learning (ML) techniques have been explored for accelerating elastoplastic algorithms. One such method includes replacing a part of the algorithm with an ML model which is called the "hybrid" approach. One of the most commonly used algorithms for ductile materials is the J2-based von Mises hardening elastoplasticity. To improve the performance of this model, an ML-based hybrid algorithm was sought. In this algorithm, the expensive iterative plastic correction step was replaced with a single-step prediction from a SINDY-inspired sparse nonlinear regression model. As a result, a novel Sparse Identification of Plastic Strain-increment (SIPS) based hybrid von Mises hardening plasticity model was formulated. This SIPS model was trained to predict the plastic strain increment from the trial stress and the unit outward normal to the yield surface at every timestep. The training data comprised loading, unloading and cyclic loading scenarios for randomly sampled numerous hardening parameters. This allowed the hybrid model to be applicable to a wide range of materials. The SIPS-based material model was then programmed in LS-DYNA® via the User Defined Material feature to conduct benchmark FE simulations. The proposed hybrid-SIPS model achieved up to 95% accuracy on standard tests and 3D simulations. Notably, it displayed an average computational cost reduction of 40%. By exploring this approach extensively, it is possible to develop universal and inexpensive hybrid material models.

Keywords: Machine Learning, Elastoplasticity, Material model, Finite Element Method

## 2 Introduction

In Finite Element (FE) simulations, material models are evaluated multiple times for each element in the domain for every timestep in the simulation. The empirical models currently used to define material behavior were formulated in the 1800s. For example, the J2 plasticity model with the von Mises yield criterion [1] for ductile materials and viscoplastic models by Perzyna [2] and Duvaut-Lions [3] are to date applied extensively in structural simulations. However, the algorithmic development of these models concerning computational cost has been lacking. This led to the notion of using Machine Learning (ML) to improve their performance.

Current research in this area has focused on mapping the relationship between stress and strain tensors. This is termed the "holistic" approach. However, the stress-strain relationship is highly intricate, and training regression or Neural Network (NN) models on it would need large data sets. Moreover, this approach does not use any valuable information gained from the classical models. This resulted in the concept of integrating the classical techniques with the capabilities of ML to form a "hybrid" model. Compared to the holistic approach, only a handful of work has been published on formulating hybrid models.

The simplest approach was executed by Palau et al. [4] in which they trained a Feedforward Neural Network (FNN) to predict the stress tensor in the J2 elastoplastic linear isotropic hardening model as a function of strain and history variables. The FNN predicted the stress state at each timestep and progressed in time. Although promising, the assumption of plane strain condition limits it to 2D elements. Also, the model was trained only for a specific material and was not generalizable. It also produced unrealistic results in multi-element simulations. It is well-known in isotropic plasticity, that the stress tensor can be represented completely in terms of principal stresses. Using this, Huang et al. [5] decomposed the principal stresses into basis vectors and coefficients using Singular Value Decomposition (SVD). They used separate FNNs to predict these decomposed principal stresses as a function of principal strains and accumulated plastic strain. Zhang and Mohr [6] trained an FNN to map the relationship between plastic dissipation and stress using a modified constitutive tensor (similar to the stiffness tensor) for Swift isotropic hardening and plane stress conditions. Flaschel et al. [7] implemented a sparse and interpretable nonlinear regression model for learning the strain energy density in hyperelastic models as a function of the Cauchy-Green strain invariants using force-displacement data obtained from FEM results. Their model was a great inspiration towards using sparse nonlinear regression for material models. Vlassis and Sun [8] proposed an interesting approach to replacing the major sections of a material model with different ANNs. Their holistic model comprised an ANN each for elastic energy, yield function and hardening law. Zhang et al. [9] formulated a hybrid FEM-NN constitutive model by leveraging the full-field data from the FEM simulations for NN training. Their ANN was trained to predict the new yield or flow stress as a function of plastic strain. Haghighat et al. [10] undertook a physics-informed approach and trained an FNN to predict the plastic multiplier as a function of time for a single material. The loss function was derived from the plastic consistency condition, KKT optimality condition, strain-stress data during training, and non-negativity constraints.

While the recent research in ML-based material models is impressive, the major drawbacks include,
- models constrained to a single material,
- plane stress or plane strain assumptions,
- restriction to rate-independent formulation,
- lack of testing on realistic FE simulations and
- lack of computational performance analysis.

To tackle these issues, we sought a generalizable ML-based material model for not one, but a wide range of materials. For the purpose of this study, the J2 plasticity model with von Mises yield criterion, nonlinear isotropic hardening, linear kinematic hardening and Perzyna viscoplasticity was chosen.

## 3 J2 plasticity model

To explain the hybrid algorithm, it is important to first recall the return mapping algorithm for the classical material model. In the small-strain deformation theory, the strain is additively split into elastic and plastic or viscoplastic parts. Plastic and viscoplastic terminology are used interchangeably in further sections. The Cauchy stress tensor is calculated using Hooke's law,

$$\bar{\sigma} = \mathbb{C} : \bar{\epsilon}^{e} = \mathbb{C} : (\bar{\epsilon} - \bar{\epsilon}^{vp}) \tag{1}$$

where the elastic stiffness tensor ($\mathbb{C}$) is defined using the Lamé parameters $\lambda$ and $\mu$

$$\mathbb{C} = \lambda\, I \otimes I + 2\mu\mathbb{I} \tag{2}$$

The Lamé parameter $\lambda$ is calculated using the bulk modulus $(\kappa)$ and shear modulus $(\mu)$ using the relationship $\lambda = \kappa - (2/3)\,\mu$. In this hypothesis, it is assumed that the material response depends on an internal variable $(\zeta)$ i.e., equivalent plastic. For hardening, the nonlinear Voce saturation law [11] in combination with linear law was considered for isotropic hardening and purely linear Prager law [12] for kinematic hardening. This led to the definition of the isotropic hardening parameter $(q)$ and the back-stress tensor $(\bar{q})$ as,

$$q = -\mathbb{K}(\zeta) = -(\sigma_{\infty} - \sigma_{Y})\left(1 - e^{-\delta\zeta}\right) - K\zeta \tag{3}$$

$$\bar{q} = \mathbb{H}(\bar{\epsilon}^{vp}) = \frac{2}{3} H\bar{\epsilon}^{vp} \tag{4}$$

Here, $H$ is the kinematic hardening modulus, $K$ is the linear isotropic hardening modulus, $\delta$ is the isotropic hardening exponent, $\sigma_{\infty}$ is the infinity stress and $\sigma_{Y}$ is the yield stress. Equation (3) uses the saturation stress $\sigma_{sat} = \sigma_{\infty} - \sigma_{Y}$. The most commonly used yield criterion is the von Mises yield function given by,

$$f(\bar{\sigma}, q, \bar{q}) = \| \, dev\, \bar{\sigma} - \bar{q} \, \| - \sqrt{\frac{2}{3}}(\sigma_{Y} - q) \tag{5}$$

The von Mises yield criterion assumes the deviatoric part of the stress tensor as the primary contributor to plastic deformation. The normal to the yield surface is then computed as,

$$\bar{n} = \frac{\partial f}{\partial \bar{\sigma}} = \frac{dev\ \bar{\sigma} - \bar{q}}{\| dev\ \bar{\sigma} - \bar{q} \|} \tag{6}$$

The deformation is elastic when the stress state lies inside the yield surface and plastic if it lies outside. The unit outward normal to the surface determines the direction of the von Mises stress propagation. Using the yield function as the plastic potential in the associative plastic flow rule, the expression for the rate of change of internal variables is obtained as,

$$\dot{\bar{\epsilon}}^{vp} = \frac{\partial f}{\partial \bar{\sigma}} = \gamma \bar{n} \tag{7}$$

$$\dot{\zeta} = \frac{\partial f}{\partial q} = \sqrt{\frac{2}{3}}\bar{n} \tag{8}$$

Using the Perzyna viscoplasticity, an expression for the plastic multiplier is given as,

$$\gamma = \frac{1}{\eta} \langle f(\bar{\sigma}, q, \bar{q}) \rangle \tag{9}$$

By allowing overstress, this model relaxes the material over a relaxation time given by,

$$\tau = \eta \left( 2\mu + \frac{2}{3}K + \frac{2}{3}H \right)^{-1} \tag{10}$$

To obtain the stress states in time, the differential equations are typically integrated using the implicit Backward Euler algorithm. The trial stress state $[\bar{\sigma}^{trial}, q^{trial}, \bar{q}^{trial}]$ is calculated at the $n^{th}$ timestep using Equations (1-4). Then, the value of the trial yield function $f^{trial}([\bar{\sigma}^{trial}, q^{trial}, \bar{q}^{trial}])$ is calculated using Equation (5). If the value is less than or equal to zero, the regime is considered elastic and the trial stresses are accepted.

$$if\ f^{trial} \leq 0, \quad [\bar{\sigma}, q, \bar{q}]_{n+1} = [\bar{\sigma}^{trial}, q^{trial}, \bar{q}^{trial}] \tag{11}$$

However, if the deformation is plastic i.e., $if\ f^{trial} > 0$, the trial stress state needs to be corrected. This is done by minimizing the residual of the plastic consistency condition with Newton-Raphson iterations.

$$Initialize\ \gamma = 0.0 \tag{12}$$

$$\begin{aligned} & for\ k = 0{:}\, n_{iter}{:} \\ & \quad g = residual\ (\gamma, \Delta t, f, \mu, \eta, \delta, K, H, \zeta, \sigma_\infty, \sigma_Y) \\ & \quad g' = \frac{\partial g}{\partial \gamma} \\ & \quad \gamma = \gamma - g/g' \end{aligned}$$

Once the plastic multiplier is obtained through the iterative procedure in Equation set (12), internal variables and stress state are updated as,

$$\bar{\epsilon}^{vp}_{n+1} = \bar{\epsilon}^{vp}_{n} + \gamma \bar{n} \Delta t \tag{13}$$

$$\zeta_{n+1} = \zeta_n + \sqrt{\frac{2}{3}}\gamma \Delta t = \sqrt{\frac{2}{3}\left( \dot{\bar{\epsilon}}^{vp}_{n+1} : \dot{\bar{\epsilon}}^{vp}_{n+1} \right)} \tag{14}$$

$$\bar{\sigma}_{n+1} = \bar{\sigma}^{trial}_{n+1} - 2\mu\gamma\bar{n}\Delta t \tag{15}$$

$$q_{n+1} = -\mathbb{K}(\zeta_{n+1}) \tag{16}$$

$$\bar{q}_{n+1} = \mathbb{H}\left( \bar{\epsilon}^{vp}_{n+1} \right) \tag{17}$$

After updating, the algorithm repeats the procedure for the next timestep. It was observed here, that the most expensive task in this procedure is the iterative projection of the stress state onto the yield surface.

## 4 Hybridization approach

The idea was thus to replace the plastic projection with a single prediction from an ML model for a range of material hardening parameters. To do that, it was necessary to find appropriate inputs to the model which would predict the plastic strain increment or correction. In the notion of radial return mapping, once the material enters the plastic regime the trial state is no longer purely elastic. It depends on the plastic strain and internal variables which are now non-zero. This implies that the evolution of trial stress itself depends on material hardening and viscoplastic response. Similarly, the unit outward normal to the yield surface also depends on the internal variables. This means that;

*For different material hardening, the trial stresses and unit outward normal evolve differently*.

This discovery was crucial for this model. To visualize it, the evolution of $xx$-component of the normalized trial stress was plotted for three different isotropic hardening moduli when subjected to an axial loading-unloading-loading path. It can be seen in Fig. 1 that, once the elastic regime ends, the stress paths diverge based on their respective hardening and viscoplastic behavior.

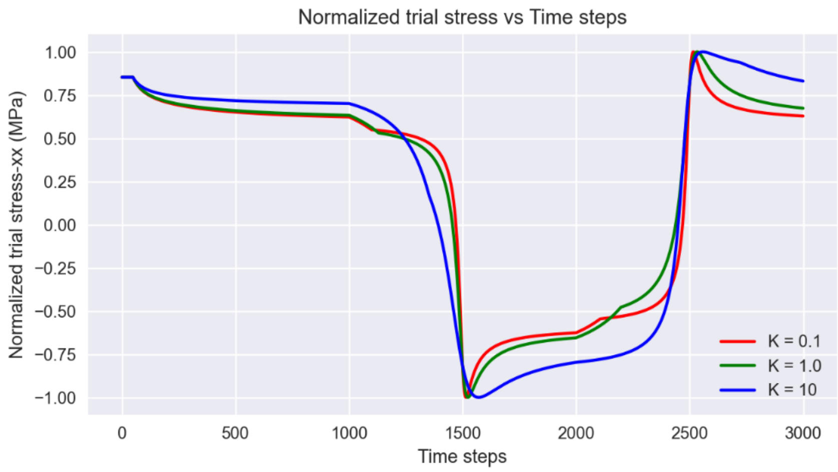


*Fig.1: Trial stress $\bar{\sigma}_{xx}^{trial}$ for different isotropic hardening modulus*

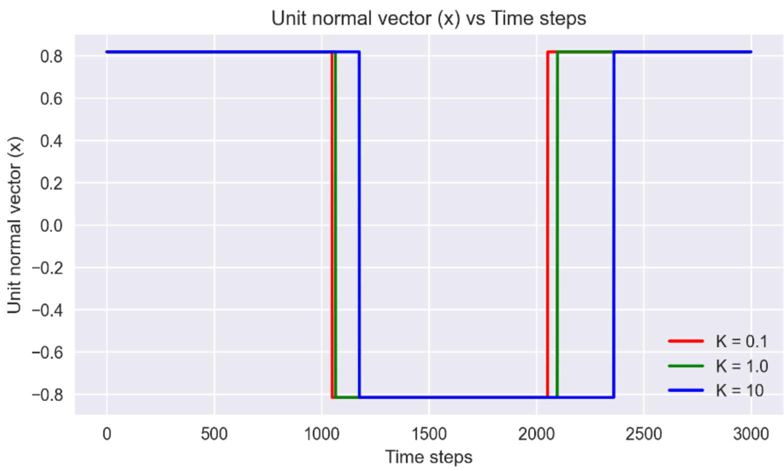


*Fig.2: Unit outward normal $\bar{n}_{xx}$ for different isotropic hardening modulus*

Similarly, the evolution of $xx$-component of the unit outward normal is shown in Fig. 2. Due to this effect, it was inferred that the underlying effects of plasticity are embedded in the trial stress and the normal vector at each timestep. It is thus possible to extract this information and predict the necessary plastic correction. Thus, the trial stresses and unit outward normal were chosen as model inputs. To reduce the input dimensionality, the trial stress tensor was represented by its principal components $(\sigma_1^{trial}, \sigma_2^{trial}, \sigma_3^{trial})$. Additionally, since the unit outward normal is a symmetric tensor, the Voigt notation was adopted.

This led to the selection of model inputs as,

$$\bar{x} = \left[\sigma_1^{trial}\ \ \sigma_2^{trial}\ \ \sigma_3^{trial}\ \ \bar{n}_{xx}\ \ \bar{n}_{yy}\ \ \bar{n}_{zz}\ \ \bar{n}_{xy}\ \ \bar{n}_{yz}\ \ \bar{n}_{zx}\right] \tag{18}$$

It is important to note that the principal trial stresses were normalized by dividing it with its Euclidean norm $\sqrt{\left(\sigma_1^{trial}\right)^2 + \left(\sigma_2^{trial}\right)^2 + \left(\sigma_3^{trial}\right)^2}$. This removed the dependency on the magnitude of stress. The plastic strain rate or, algorithmically, the plastic strain increment $(\dot{\bar{\epsilon}}^{vp} = \Delta\bar{\epsilon}^{vp} = \gamma\bar{n})$ was chosen as the output. It was found that predicting the scalar plastic multiplier $(\gamma)$ instead was not as effective due to a lack of information on directions. Thus, the model outputs were,

$$\bar{y} = \left[\Delta\epsilon_{xx}^{vp}\ \ \Delta\epsilon_{yy}^{vp}\ \ \Delta\epsilon_{zz}^{vp}\ \ \Delta\epsilon_{xy}^{vp}\ \ \Delta\epsilon_{yz}^{vp}\ \ \Delta\epsilon_{zx}^{vp}\right] \tag{19}$$

## 5 ML modeling

The ML modeling approach was thus finalized as,

$$\left[\sigma_1^{trial}\ \ \sigma_2^{trial}\ \ \sigma_3^{trial}\ \ \bar{n}_{xx}\ \ \bar{n}_{yy}\ \ \bar{n}_{zz}\ \ \bar{n}_{xy}\ \ \bar{n}_{yz}\ \ \bar{n}_{zx}\right] \Rightarrow \boxed{\text{ML}} \Rightarrow \left[\Delta\epsilon_{xx}^{vp}\ \ \Delta\epsilon_{yy}^{vp}\ \ \Delta\epsilon_{zz}^{vp}\ \ \Delta\epsilon_{xy}^{vp}\ \ \Delta\epsilon_{yz}^{vp}\ \ \Delta\epsilon_{zx}^{vp}\right]$$

After predicting the strain increment, the internal variables and stress state can be updated using Equations (13-17). To generate the training data, the classical von Mises return mapping algorithm was run on synthetic loading, unloading, and cyclic loading strain paths for random strain magnitudes, strain rates, and material hardening parameters within a specific range. The parameter ranges are shown in Table 1.

| $\boldsymbol{\epsilon}$ | $\boldsymbol{K}$ | $\boldsymbol{H}$ | $\boldsymbol{\delta}$ | $\boldsymbol{\Delta t}$ | $\boldsymbol{\eta}$ |
|---|---|---|---|---|---|
| $[-0.1, 0.1]$ | $[0, 1]\ GPa$ | $[0, 1]\ GPa$ | $[0, 50]$ | $[1e^{-5}, 1e^{-3}]\ s$ | $[0, 0.1]\ GPa.s$ |

*Table 1: Range of material and simulation parameters for training data generation*

In total, 120 strain paths consisting of 700,000 timesteps of data were generated out of which, 40,000 timesteps corresponded to the plastic regime. The inputs and outputs of the model were extracted for the plastic regime. After careful investigation of FNN, LASSO regression [13] and SINDy [14], it was found by Bokil et al. [15] that the sparse nonlinear regression method of SINDy outperformed the others. The algorithm uses ordinary least squared minimization with L2 regularization and zeroes out the coefficients below a specific threshold. This essentially forces the model to learn the true relationship between the data using the sparsest possible model. In the case of Sparse Identification of Plastic Strain rate (SIPS), the model was trained to fit the coefficients $(\bar{a})$ for the following expression,

$$\bar{y} = a_0 + \bar{a}_1 * \bar{x} + \bar{a}_2 * LeakyReLU(\bar{x}) \tag{20}$$

Where $\bar{y}$ are the model outputs and $\bar{x}$ are the model inputs. The cut-off threshold was set to 1e-5, the regularization parameter was tuned to 3e4 and the SIPS model was trained for 1000 iterations. The trained model was seen to be 27% sparse, meaning that out of the total coefficients to be optimized, 27% of the coefficients were nullified. The SIPS model attained a Mean Squared Error (MSE) of 2.8e-3 on the training data.

Finally, the trained model was plugged into the return mapping algorithm in place of the Newton-Raphson iterative procedure to predict the plastic strain increment tensor from the normalized principal trial stresses and the unit outward normal vector at each timestep. The figure below explains the hybrid algorithm.

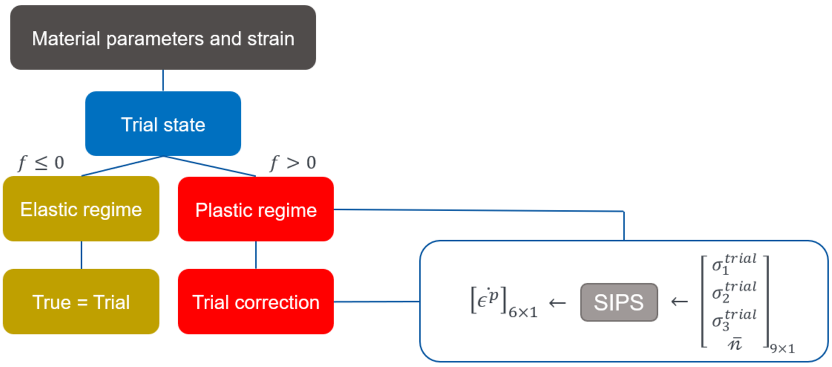


*Fig.3: A single timestep in the SIPS hybrid algorithm*

# 6 Results

The hybrid model was tested on various standard and non-standard strain paths for random material parameters. An interesting point to note is that,

*The model is virtually independent of yield stress.*

This is because it is irrelevant "when" the material yields, but "if" it yields. Once the material yields, the SIPS model is activated. The inputs are normalized by construction and the actual magnitude of the trial stresses does not affect the model. This hypothesis was checked in a test shown in Section 6.3. Since the model was trained on selected hardening parameters, the remaining material parameters in Table 2 were kept constant for the tests.

| $\boldsymbol{\kappa}$ | $\boldsymbol{\mu}$ | $\boldsymbol{\sigma_Y}$ | $\boldsymbol{\sigma_\infty}$ | $\boldsymbol{\Delta t}$ |
|---|---|---|---|---|
| $17.5\ GPa$ | $8\ GPa$ | $300\ MPa$ | $2\sigma_Y$ | $1e-3\ s$ |

*Table 2: Constant material parameters for testing*

## 6.1 Uniaxial tension-compression loading

For the current test, the variable material hardening parameters are shown in Table 3. The relaxation time was calculated from Equation (10) and shown in the table for reference.

| $\boldsymbol{K}$ | $\boldsymbol{H}$ | $\boldsymbol{\delta}$ | $\boldsymbol{\eta}$ | $\boldsymbol{\tau}$ |
|---|---|---|---|---|
| $0.1\ GPa$ | $0.1\ GPa$ | $25$ | $1e8\ Pa\ s$ | $4.7e-3\ s$ |

*Table 3: Material parameters for uniaxial tension-compression*

The strain path was a pure axial loading-unloading-loading condition, as shown in Fig 4.

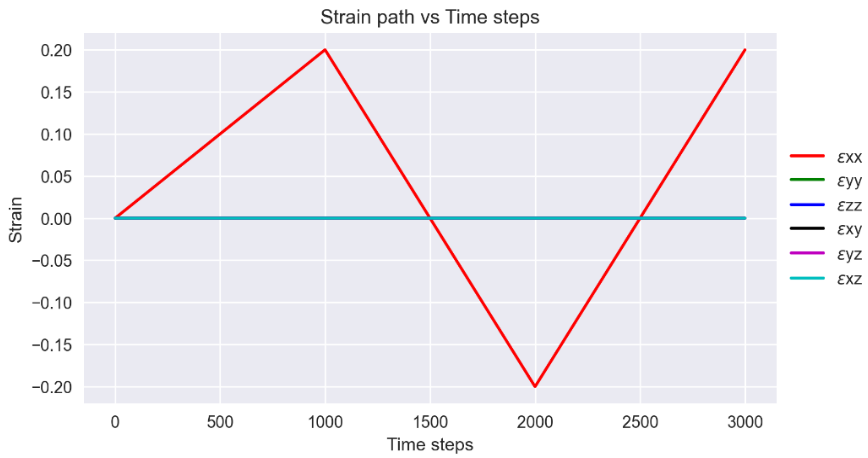


*Fig.4: Uniaxial loading-unloading-loading strain path*

It should be noted here that the strain magnitude was between [-0.2, 0.2] which was outside the training range of the model. This strain path causes a strain rate for the first 1000 steps to be 0.1 /s, between 1000-2000 steps to be 0.2 /s and from 2000-3000 steps to again be 0.1 /s. After simulating this strain path using the classical von Mises model and the hybrid SIPS model, the final stresses were compared. As the loading is purely axial, the principal stresses (same as axial stresses) and effective plastic strain were compared as shown in Fig. 5 and Fig. 6.

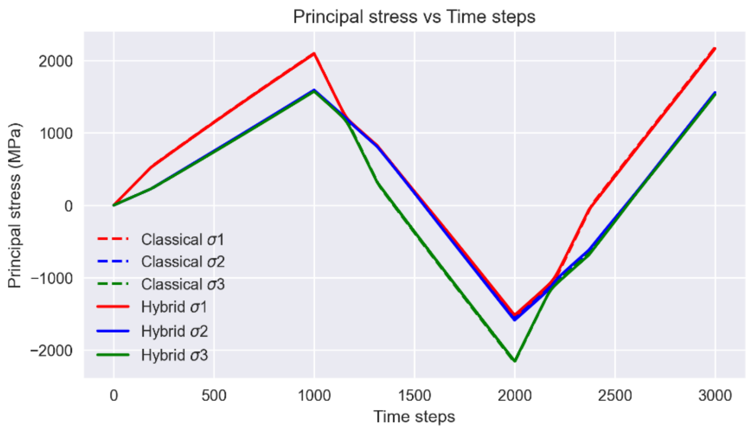


*Fig.5: Comparison of principal stresses (load-unload-load)*

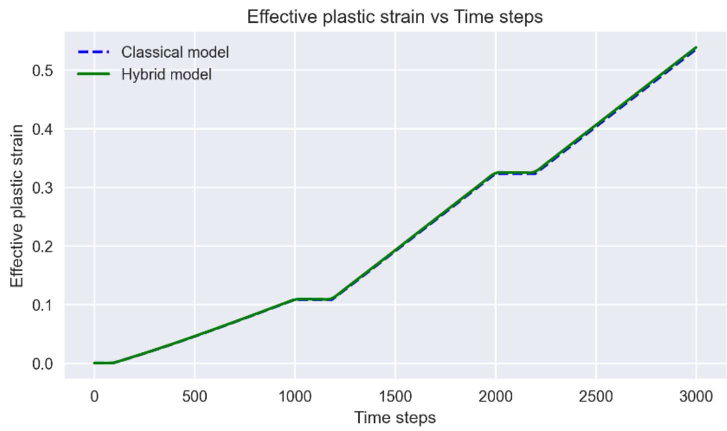


*Fig.6: Comparison of effective plastic strain (load-unload-load)*

The principal stresses and effective plastic strain from the hybrid model completely agree with the classical model. The Mean Absolute Percentage Error (MAPE) ranged between 1-6 %. Fig. 7 displays the comparison of the von Mises stresses.

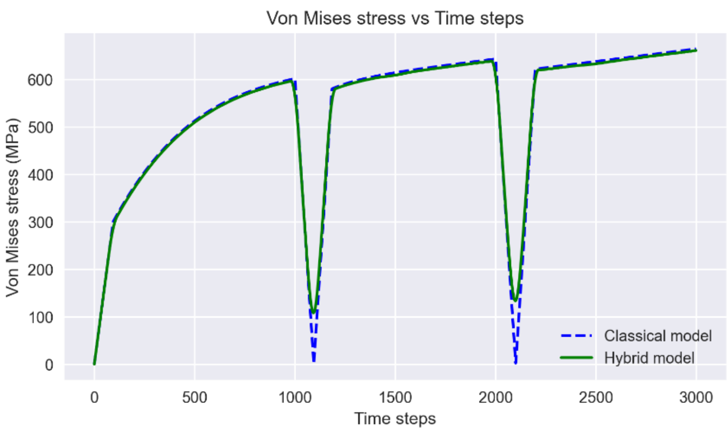


*Fig.7: Comparison of von Mises stress (load-unload-load)*

Despite high accuracy in principal stresses, the model failed to estimate the von Mises stress at certain locations with the same accuracy. It was observed that the locations of zero von Mises stress corresponded to the locations where the principal stresses intersected and had the same magnitude. Recalling the definition of von Mises stress,

$$\sigma_{VM} = \sqrt{0.5((\sigma_{11} - \sigma_{22})^2 + (\sigma_{22} - \sigma_{33})^2 + (\sigma_{33} - \sigma_{11})^2) + 3(\sigma_{12}^2 + \sigma_{23}^2 + \sigma_{31}^2)} \quad (21)$$

if the shear stresses are zero, and axial stresses are equal to each other the von Mises stress is also zero. In the hybrid model, due to errors in predicting the strain increment, the axial stresses do not cancel out completely nor the shear stresses are exactly zero. Instead, the errors get squared and added.

*In the case of zero von Mises stress, the hybrid model suffers from non-zero stress estimation*.

If these locations are ignored, the error in von Mises stress comes down to 5%. This effect was also seen in other test cases comprising load reversal. Regarding the computational time, the classical model took 0.73 seconds and the hybrid model took 0.43 seconds to complete, achieving a 40% speed-up.

## 6.2 Uniaxial cyclic loading

A cyclic loading case makes it possible to analyze the model on kinematic hardening behavior. To check the Bauschinger effect [16] clearly, a higher kinematic hardening modulus was chosen. The variable material parameters for this test are shown in Table 4.

| $K$ | $H$ | $\delta$ | $\eta$ | $\tau$ |
|---|---|---|---|---|
| $0.5\ GPa$ | $1.0\ GPa$ | $50$ | $1e6\ Pa\ s$ | $4.4e-5\ s$ |

*Table 4: Variable material parameters for cyclic loading test*

The strain path is shown in Fig. 5 and the maximum strain rate was as high as 3.2 /s.

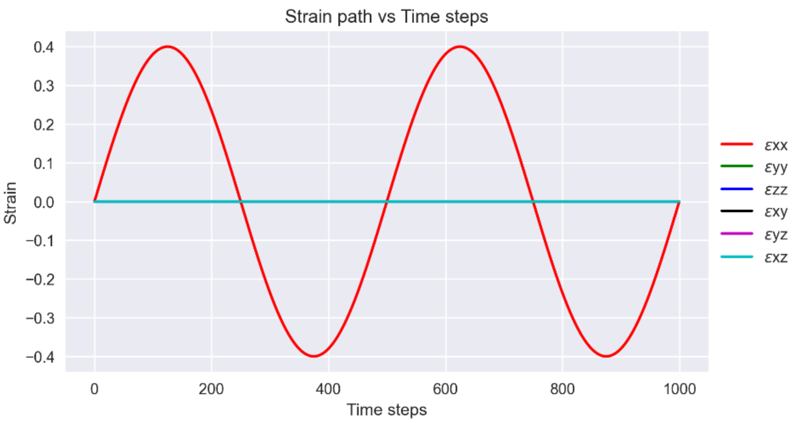


*Fig.8: Uniaxial cyclic loading strain path*

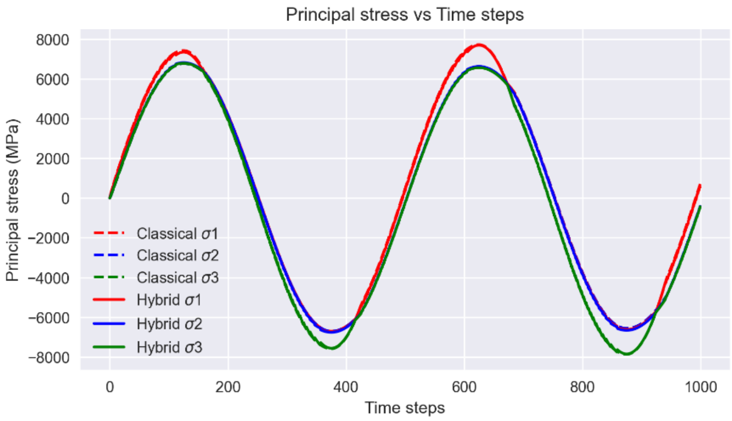


*Fig.9: Comparison of principal stresses (cyclic loading)*

In this case, the strain was further increased to 0.4 to check the model extrapolation capability. After running both models on the cyclic loading path, the stresses and plastic strain were compared as shown in Fig. 9 and Fig. 10 respectively. The maximum MAPE for principal stresses and effective plastic strain was 4%.

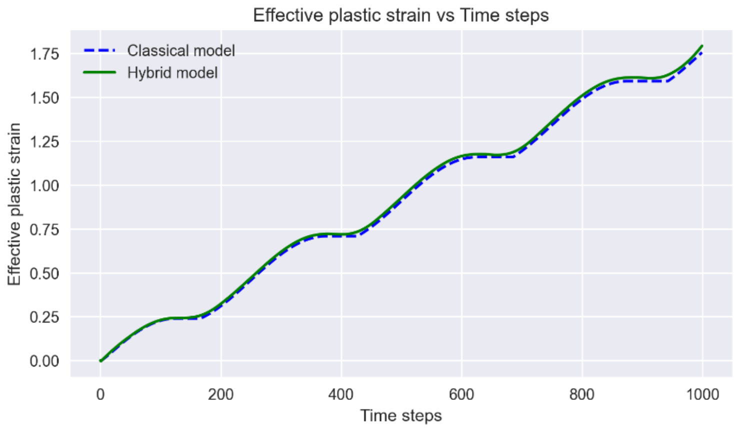


*Fig.10: Comparison of effective plastic strain (cyclic loading)*

Fig. 11 displays the comparison of von Mises stresses. The maximum MAPE for von Mises stress was 23%. Similar to the previous test, the zero von Mises stress was predicted as non-zero. Due to extreme extrapolation, minor fluctuations in the shear components (thus von-Mises stress) are also seen.

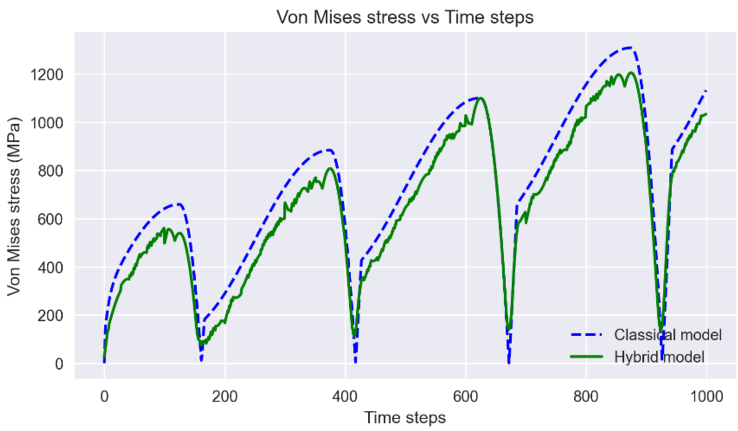


*Fig.11: Comparison of von Mises stress (cyclic loading)*

To understand the kinematic hardening behavior, the $xx$-component of the deviatoric stress tensor was plotted against the $xx$-component of the strain tensor for both the models.

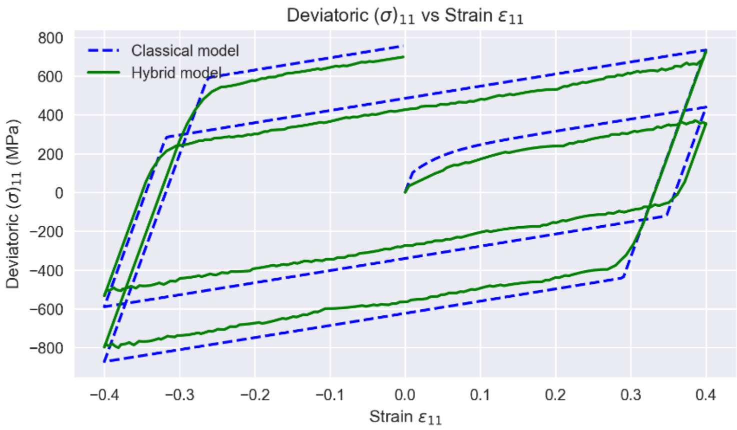


*Fig.12: Comparison of deviatoric stress (cyclic loading)*

The Bauschinger effect can be clearly seen in this plot. As the material experiences cyclic loading, it causes asymmetrical strain hardening between tensile and compressive paths. This effect has been captured by the hybrid model, although with a 10% error due to errors in shear components of the plastic strain. However, the model extrapolated without any blunders. The classical model required 0.24 seconds and the hybrid model required 0.182 seconds for stress estimation, thus achieving a cost reduction of 24%.

## 6.3 Complete loading-unloading

Another interesting test that was selected for studying was the loading-unloading-loading for all components of the strain tensor i.e., axial and shear simultaneously. The variable parameters for this test are shown in Table 5.

| $K$ | $H$ | $\delta$ | $\eta$ | $\tau$ | $\sigma_Y$ |
|---|---|---|---|---|---|
| $0.2\ GPa$ | $0.2\ GPa$ | $30$ | $1e6\ Pa\ s$ | $4.7e-5\ s$ | $500\ MPa$ |

*Table 5: Variable material parameters for complete loading test*

In this test, the yield stress was also increased to check the hypothesis of its independence on the model. The strain path for this test is shown in Fig. 13.


*Fig.13: Strain path for complete loading-unloading-loading*

In this test case as well, the strains were outside the model training range and the strain rate was observed to be between 0.06 and 0.4 /s. After running the hybrid and classical models on this strain path, the effective plastic strain and all the Cauchy stress components were compared and are shown in Fig. 14 and Fig. 15 respectively.

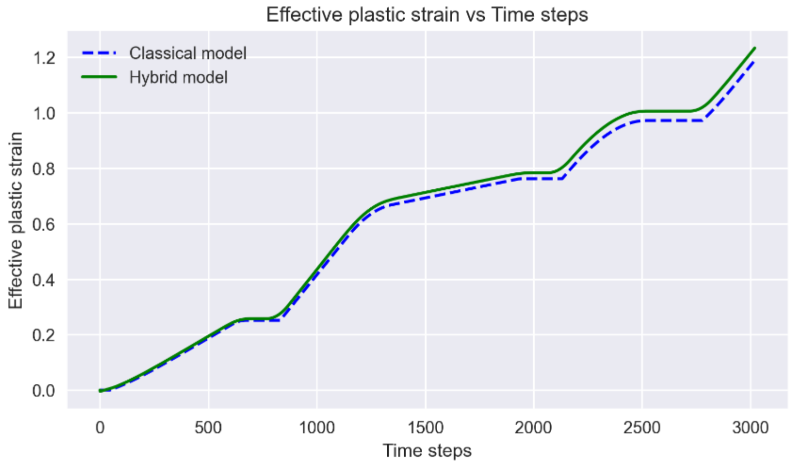


*Fig.14: Comparison of effective plastic strain (complete loading)*

The effective plastic strain was accurately predicted, as also seen in previous test. The error in the Cauchy stress tensor was less than 10%. The $\sigma_{xy}$ component was exactly 0.0 as per the classical model but was predicted slightly non-zero by the SIPS model.

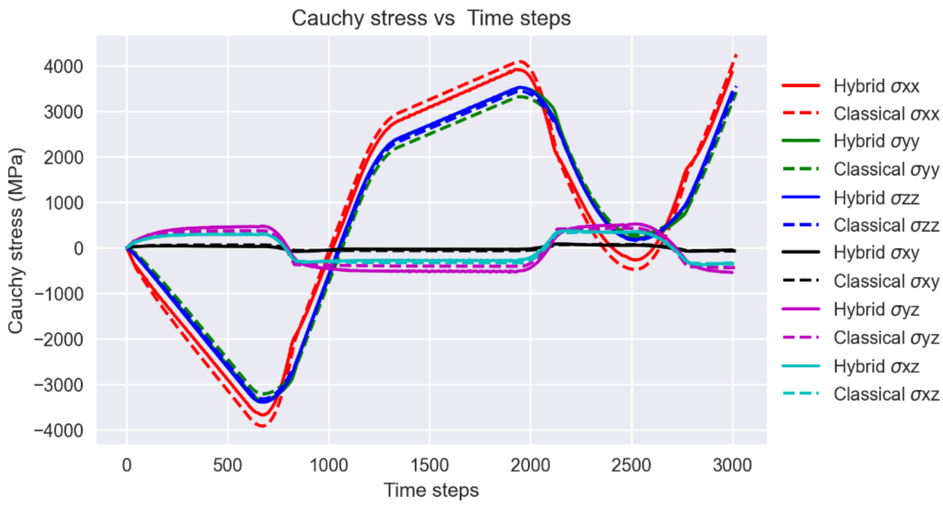


*Fig.15: Comparison of Cauchy stress (complete loading)*

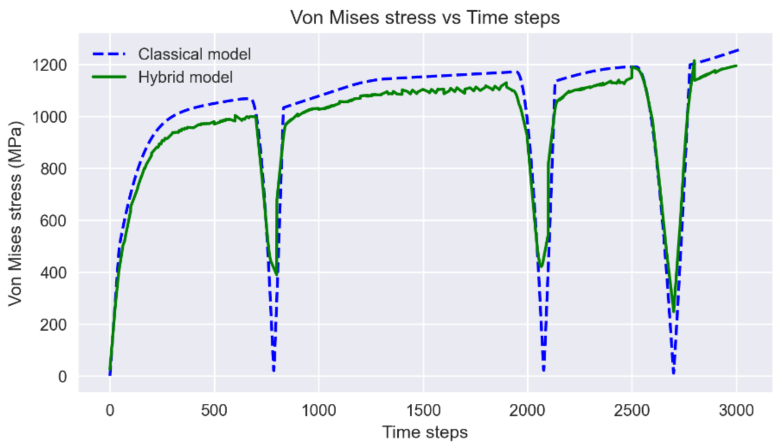


*Fig.16: Comparison of von Mises stress (complete loading)*

The error in von Mises stress is higher in this test case due to unequal axial stress components and non-zero shear stresses. It can be seen in Fig. 16 that the point in time for zero von Mises stress corresponds to equal axial stresses and zero shear stresses in Fig. 15. In this case, the hybrid model performed 41% faster than the classical model.

The combined inference of the standard tests was that the hybrid model was able to predict the material behavior with nearly 95% accuracy in effective plastic strain and principal stresses. However, in cases of exact equality in axial stresses or zero stresses, the errors led to non-physical results in von Mises stress. The overall accuracy for von Mises stress was 85%. In reality, the strain paths are not as simple. Hence, FE simulations were also carried out as a part of the tests. The next section shows the performance of the hybrid model on two benchmark simulations in LS-DYNA. For fair comparison, both, the classical and hybrid, models were programmed in LS-DYNA as User Defined Materials [17].

## 6.4 Cook's membrane simulation

The Cook's membrane is a common benchmark problem for testing FE software and material models. The 3D geometry and boundary conditions were defined in LS-PrePost and are shown in Fig. 17 below. The problem comprised of a cantilever plate with a fixed support subjected to prescribed displacement at the edge. The FE model contained 186 hexahedral first-order elements and 285 nodes. Due to computational limitations to the Python-based custom material models, a relatively coarse mesh was used. However, the performance of the hybrid model is independent of number of elements.

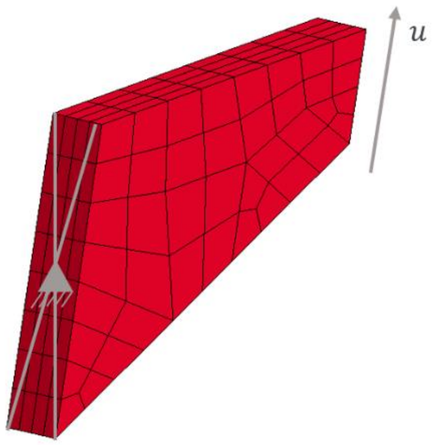


*Fig.17: Problem definition of Cook's membrane*

The material and simulation parameters for this test were as follows:

| $\kappa$ | $\mu$ | $\sigma_Y$ | $\sigma_\infty$ | $\mathbf{K}$ |
|---|---|---|---|---|
| $17.5\ GPa$ | $8\ GPa$ | $200\ MPa$ | $2\sigma_Y$ | $0.5\ GPa$ |

| $H$ | $\delta$ | $\eta$ | $\Delta t$ | $\mathrm{T_{end}}$ |
|---|---|---|---|---|
| $0.5\ GPa$ | 20 | $1e7\ Pa\ s$ | $9.9e-4\ s$ | $4.0\ s$ |

*Table 6: Material and simulation parameters for Cook's membrane*

By running the models on this simulation, the contour plots for results at the end time were compared and are shown below.

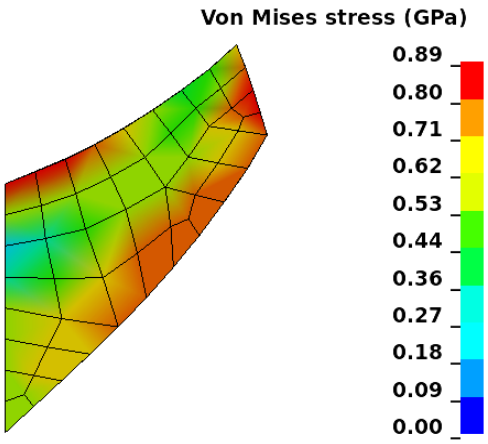


*(a) Classical model*

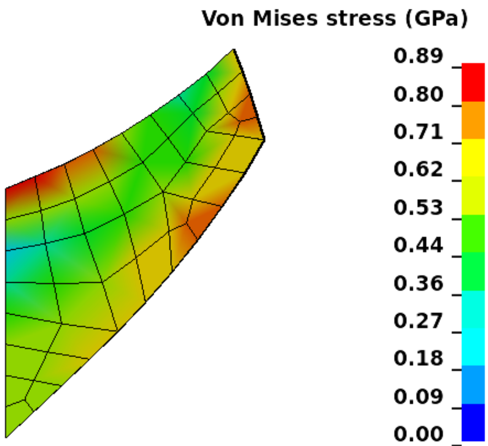


*(b) Hybrid model*

*Fig.18: Comparison of von Mises stress contour (Cook's membrane)*

Visibly, the result from the hybrid model was in good agreement with that from the classical model. The maximum von Mises stress was correctly estimated. The stress response at the top edge and the right edge of the membrane was quite accurate, but the high-stress region due to bending at the bottom edge was slightly underpredicted. To compare the material behavior at these critical locations, the effective plastic strain was plotted for elements at the left edge (A), bottom edge (B), top edge (C) and right edge (D) of the plate.

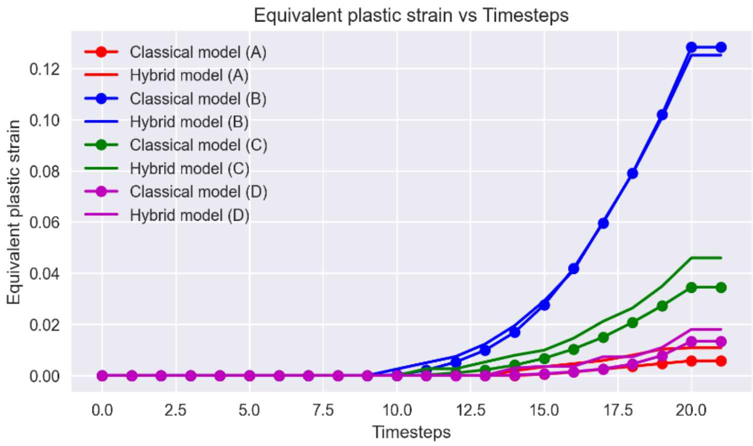


*Fig.19: Comparison of effective plastic strain (Cook's membrane)*

While the MAPE for element (B) was 3%, the same for (A), (C) and (D) was around 20%. Theoretically, the plastic strain is not unique to the stress. Different plastic strains can indeed lead to the same stress behavior. Hence, technically the plastic strain from the hybrid model was not completely inaccurate. To quantitively understand the performance of the hybrid model in the FE simulation, a plot of the percentage error in time for all elements was generated.

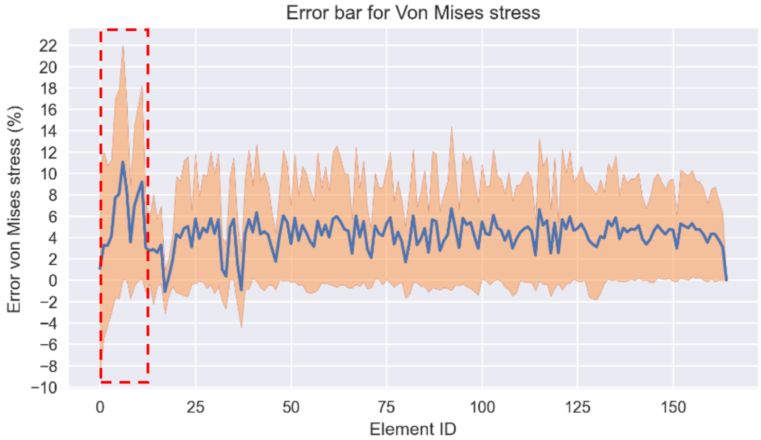


*Fig.20: Percentage error plot for all elements (Cook's membrane)*

The maximum and minimum percentage error in time for each element can be seen in Fig. 20. For 85% of the elements in the model, the MAPE was 4% with a standard deviation of $\pm$ 6%. The elements from ID 0-15 showed an error of more than 20%. However, this plot individually can be misleading.

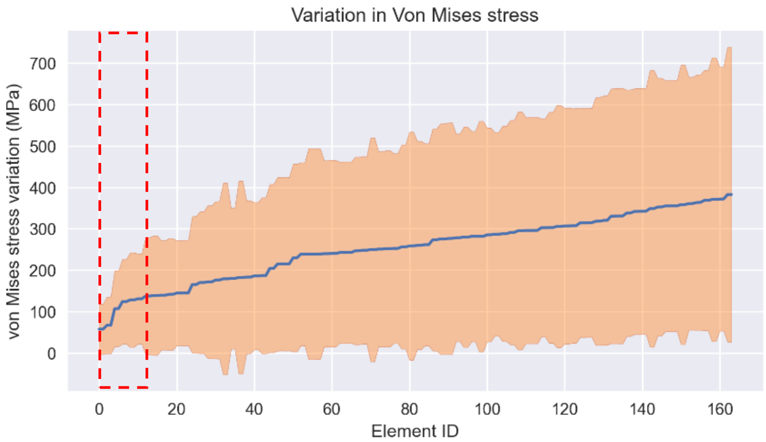


*Fig.21: Variation of von Mises stress in elements (Cook's membrane)*

The shaded region in Fig. 21 shows the range of von Mises stress for each element in time and the mean von Mises stress is plotted on top of it. The elements from ID 0-15, which have a higher MAPE, correspond to a small MAE (10-30 MPa) and stress magnitude (100-200 MPa) which are insignificant in causing plastic failure. It was also verified that the error did not propagate in time and the standard deviation remained bounded.

In particular, the classical model required 446 seconds to complete the simulation while the hybrid model performed it in 213 seconds, thus achieving an acceleration of 52%.

## 6.5 Cyclically loaded tube simulation

In this simulation, a tube was subjected to axial cyclic loading. This induced axial, shear and bending stresses in the geometry which can be used to assess the hybrid model better. The FE model was created in LS-PrePost as shown below.

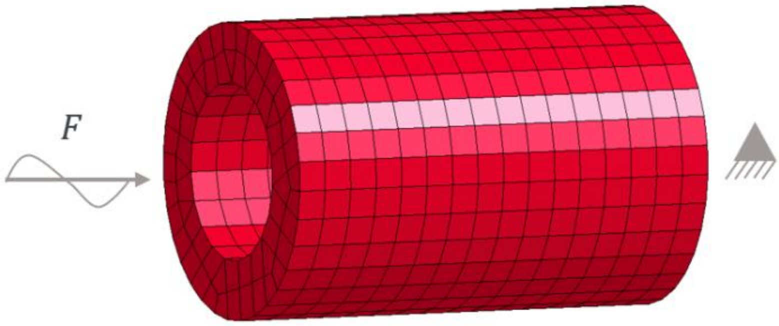


*Fig.22: Problem definition of cyclically loaded tube*

The tube was subjected to a cyclic loading curve shown in Fig. 23.

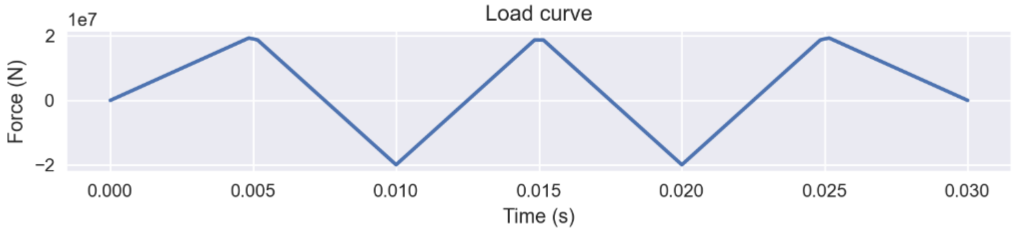


*Fig.23: Cyclic load curve imposed on the tube*

The material and simulation parameters for this test were as follows:

| $\kappa$ | $\mu$ | $\sigma_Y$ | $\sigma_\infty$ | $\mathbf{K}$ |
|---|---|---|---|---|
| $17.5\ GPa$ | $8\ GPa$ | $300\ MPa$ | $2\sigma_Y$ | $1.0\ GPa$ |

| $H$ | $\delta$ | $\eta$ | $\Delta t$ | $\mathrm{T_{end}}$ |
|---|---|---|---|---|
| $0.8\ GPa$ | 50 | $1e8\ Pa\ s$ | $1.7e-5\ s$ | $0.03\ s$ |

*Table 7: Material and simulation parameters for cyclically loaded tube*

After completing the simulation, the von Mises stress contour at the end was compared, as shown in Fig. 24. In these contour plots, the accurate correlation between the models is clear. The hybrid model predicted the plastic increments correctly and thus estimated the final stress state as precise as the classical model.

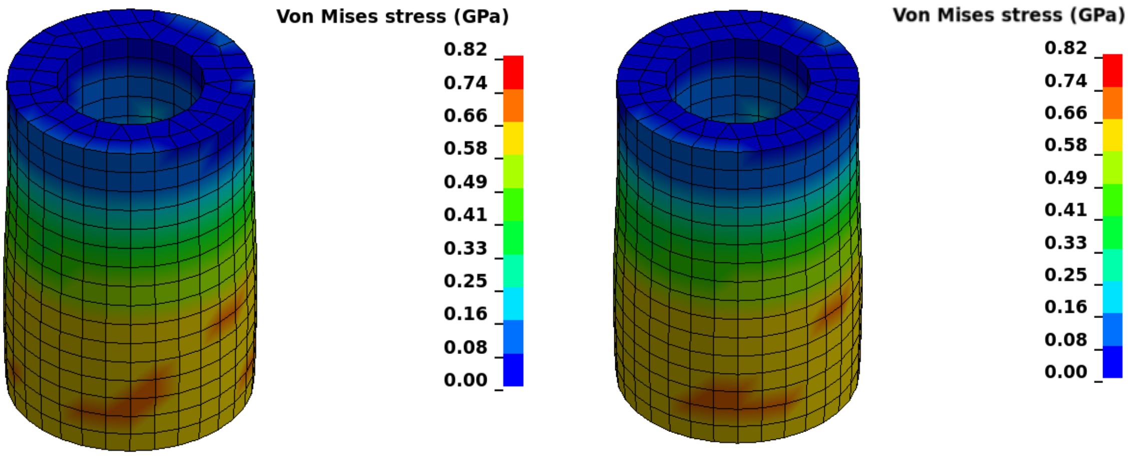


*(a) Classical model* *(b) Hybrid model*

*Fig.24: Comparison of von Mises stress contour (cyclically loaded tube)*

To visualize the behavior of the material model at different locations in the geometry, the effective plastic strain is plotted for an element in the bottom zone (A), in the middle zone (B) and, in the top zone (C) of the tube.

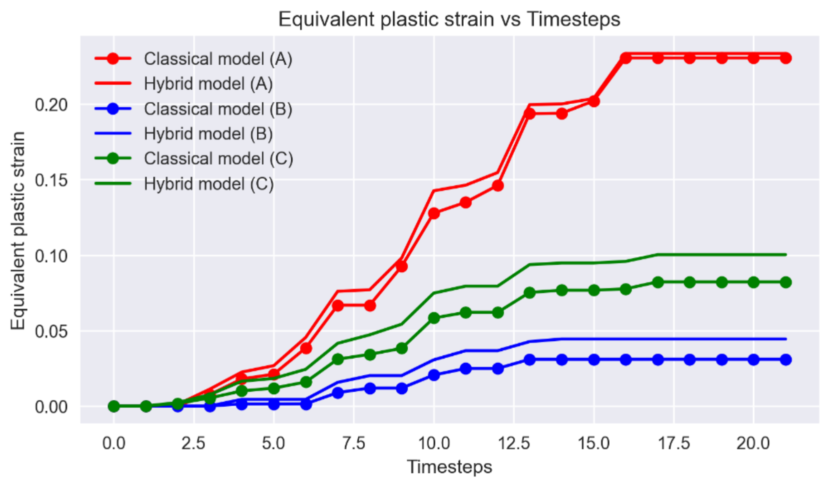


*Fig.25: Comparison of effective plastic strain (cyclically loaded tube)*

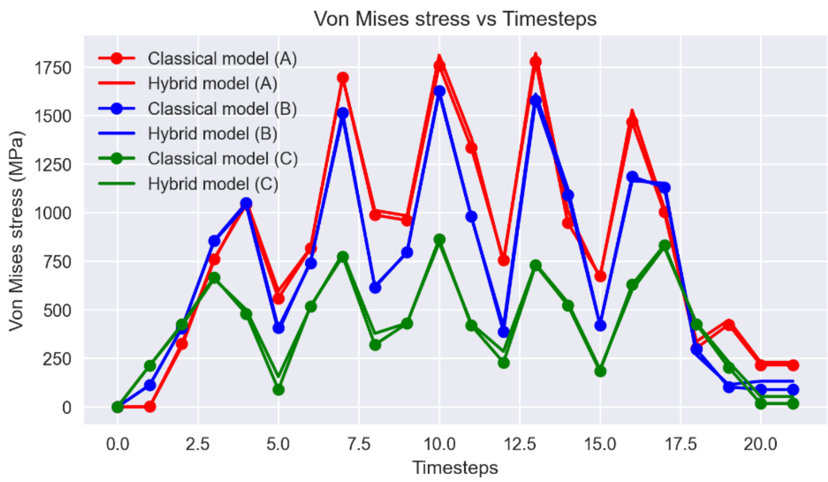


*Fig.26: Comparison of von Mises stress (cyclically loaded tube)*

From Fig. 25, it was observed that the MAPE for elements (B) and (C) was 25% and element (A) was 10%. Here as well, since the plastic strain is not unique to the stress. Even if there was a large difference in the plastic strain, it resulted in the same von Mises stress as the classical model. In Fig. 26, the accuracy of the model in terms of von Mises stress is clearly observed. The total MAPE for all elements in von Mises stress was 10%. The figure below shows the percentage error bar for all elements throughout simulation time.


*Fig.27: Percentage error plot for all elements (cyclically loaded tube)*

For 92% of the elements in the model, the mean percentage error was 2% with a standard deviation of $\pm$ 10%. Similar to the Cook's membrane simulation, the elements with larger errors from ID 0-30 correspond to smaller values of stress as seen below.

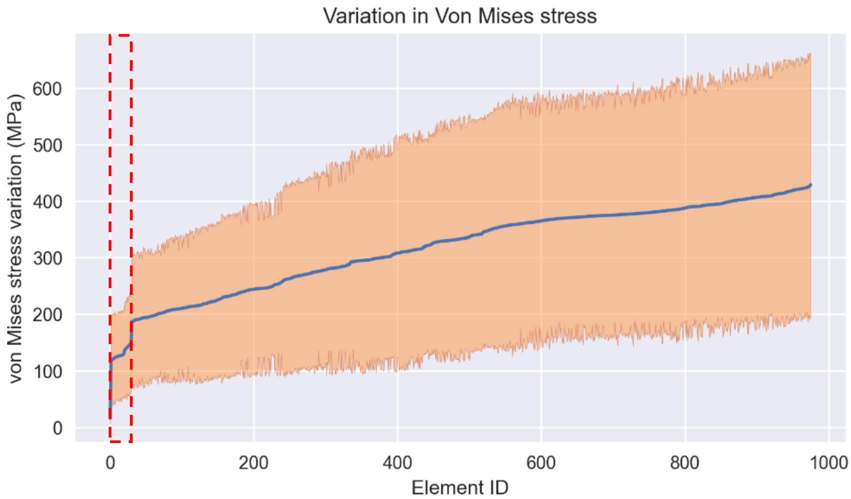


*Fig.28: Variation of von Mises stress in elements (cyclically loaded tube)*

For the first 30 elements, the mean von Mises stress was approximately 180 MPa. These elements do not contribute to the plastic failure. A 25% error in these elements corresponds to 45 MPa. On the other hand, the elements that undergo larger plastic deformation and stresses were estimated with a 90% accuracy.

The computation time for the classical model was 1665 seconds while the same for the hybrid model was only 606 seconds, thus attaining a 63% cost reduction.

In the FE simulations, the SIPS model estimated the von Mises stress with higher accuracy due to the absence of zero von Mises stress situations seen in standard tests. In order to analyze the hybrid model quantitatively on the strain paths and FE simulations together, the accuracy and computational cost reduction for all the tests were compared.

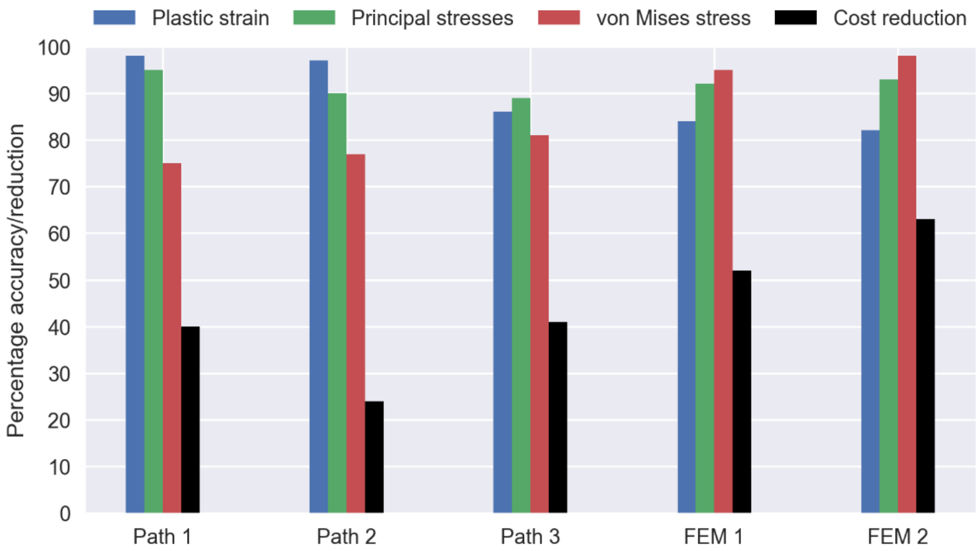


*Fig.29: Hybrid model performance analysis*

The hybrid model performed with 90% accuracy in predicting plastic strain and further estimating the principal stresses. Regarding the von Mises stresses, the model performed slightly poorly with an accuracy of 80% and minor instabilities. However, the hybrid model provided a cost reduction in the range of 20 to 60 %.

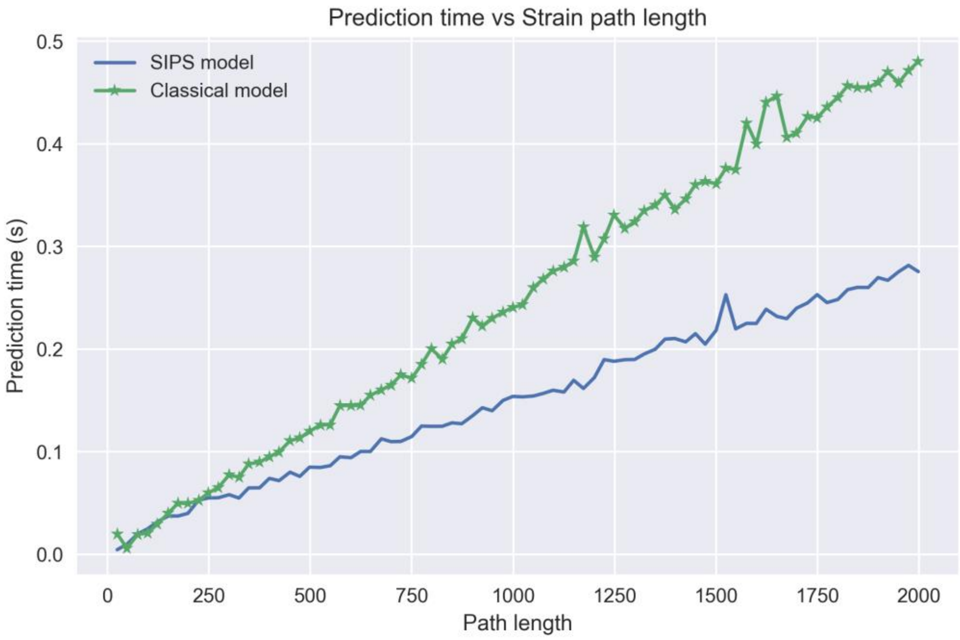


*Fig.30: Comparison of computational cost scaling*

The time taken by the hybrid and the classical model to complete the computation for an increasing number of strain path steps was measured. It was found that the cost of classical model scales with $\mathcal{O}(3N)$ and that of hybrid model scales with $\mathcal{O}(N)$. This is because the classical model needs on average 3 iterations to converge to the solution of the plastic multiplier, while the hybrid model predicts it in one shot. This was also verified in the observed cost reduction in the FE simulations.

## 7 Summary

As the FE models get larger and larger, there is a growing demand for faster simulations. In structural simulations, material models are evaluated at every timestep for every integration point in every element in the model. This leads to millions or even billions of algebraic computations and hence is thus highly expensive. Normally, high-fidelity simulations take 8-24 hours to complete. To tackle this problem from a solid mechanics point of view, a machine-learning-based approach was sought to accelerate the material model.

For this purpose, the commonly used J2 hardening plasticity model was selected. In the return mapping algorithm, the iterative plastic projection is the most expensive operation. Thus, an ML model was formulated that would perform the plastic correction in a single step using the information from the trial states. After careful investigation, the SINDy-inspired sparse nonlinear regression method was selected. Thus, a Sparse Identification of Plastic Strain-rate (SIPS) model was developed which predicted the plastic strain increment or correction using the normalized principal trial stresses and the unit outward normal vector to the yield surface at every timestep. The model was trained only on synthetic uniaxial, biaxial, and triaxial loading scenarios for a wide range of variable material parameters.

By replacing the iterative plastic projection procedure with the SIPS model and keeping the elastic regime classical, a hybrid material model was formulated. This hybrid model was also generalizable to various materials without needing additional training. Moreover, the model extrapolated very well for larger strains without any exploding errors. This was possible due to the sparsity-promoting algorithm which enabled the learning of underlying physics and preventing overfitting.

The hybrid model was tested on three specific strain paths and two FE simulations in LS-DYNA. The observations revealed that the hybrid model performed with 90-95% accuracy on principal stresses and effective plastic strain along with 80-85% accuracy on von Mises stress. Notably, the hybrid model was found to be 20-60% faster than the classical model.

Thus, if a 10-15% accuracy in a preliminary design phase can be sacrificed, a 60% speed-up would mean a reduction of computation time from 8 hours to roughly 3 hours with the hybrid model. Moreover, it was also observed that the results of the hybrid model never “blew up”. As opposed to Newton’s iterative method, the hybrid model does not suffer from convergence issues and presents an approximate result without needing iterations. Such a hybrid model would be highly instrumental in performing multiple preliminary simulations in the initial design phase. It would collectively save a substantial amount of time and effort in optimizing industrial, automobile and aerospace components.

The critical aspect of the future work will include the addition of a physics-informed loss function to tackle the issues with zero von Mises stress scenarios. As a whole, the sparse nonlinear regression displayed significant potential in accelerating the elastoplastic material model algorithms. Such an approach can also be applied to hyperelastic or complex polymer models to improve their computational performance. More extensive and physics-based training is expected to lead to a true ML-based hybrid model independent of the material parameters and thus open new doors to material modelling.

## 8 Literature


[1] R. v. Mises, “Mechanik der festen Körper im plastisch- deformablen Zustand,” *Nachrichten von der Gesellschaft der Wissenschaften zu Göttingen, Math. Klasse*, vol. 1913, pp. 582–592, 1913, [Online]. Available: http://eudml.org/doc/58894

[2] W. Olszak and P. Perzyna, “On thermal effects in viscoplasticity,” *Zeitschrift für Angew. Math. und Phys. ZAMP 1969 205*, vol. 20, no. 5, pp. 676–680, Sep. 1969, doi: 10.1007/BF01590623.

[3] G. Duvaut and J. L. Lions, “Les inéquations en mécanique et en physique,” 1972.

[4] T. Palau, A. Kuhn, S. Nogales, H. J. Böhm, and A. Rauh, “A neural network based elasto-plasticity material model,” *ECCOMAS 2012 - Eur. Congr. Comput. Methods Appl. Sci. Eng. E-b. Full Pap.*, no. Eccomas, pp. 8861–8870, 2012.

[5] D. Huang, J. N. Fuhg, C. Weißenfels, and P. Wriggers, “A machine learning based plasticity model using proper orthogonal decomposition,” *Comput. Methods Appl. Mech. Eng.*, vol. 365, pp. 1–33, 2020, doi: 10.1016/j.cma.2020.113008.

[6] A. Zhang and D. Mohr, “Using neural networks to represent von Mises plasticity with isotropic hardening,” *Int. J. Plast.*, vol. 132, p. 102732, 2020, doi: 10.1016/j.ijplas.2020.102732.

[7] M. Flaschel, S. Kumar, and L. De Lorenzis, “Unsupervised discovery of interpretable hyperelastic constitutive laws,” *Comput. Methods Appl. Mech. Eng.*, vol. 381, p. 113852, 2021, doi: 10.1016/j.cma.2021.113852.

[8] N. N. Vlassis and W. Sun, “Component-based machine learning paradigm for discovering rate-dependent and pressure-sensitive level-set plasticity models,” *J. Appl. Mech.*, pp. 1–13, 2021, doi: 10.1115/1.4052684.

[9] Y. Zhang, Q. J. Li, T. Zhu, and J. Li, “Learning constitutive relations of plasticity using neural networks and full-field data,” *Extrem. Mech. Lett.*, vol. 52, 2022, doi: 10.1016/j.eml.2022.101645.

[10] E. Haghighat, S. Abouali, and R. Vaziri, “Constitutive model characterization and discovery using physics-informed deep learning,” 2022, [Online]. Available: http://arxiv.org/abs/2203.09789

[11] E. Voce, “A practical strain hardening function,” *Metallurgia*, vol. 51, pp. 219–226, 1955.

[12] W. Prager, “A new method of analyzing stresses and strains in work-hardening plastic solids,” 1956.

[13] R. Tibshirani, “Regression shrinkage and selection via the lasso,” *J. R. Stat. Soc. Ser. B*, vol. 58, no. 1, pp. 267–288, 1996.

[14] S. L. Brunton, J. L. Proctor, J. N. Kutz, and W. Bialek, “Discovering governing equations from data by sparse identification of nonlinear dynamical systems,” *Proc. Natl. Acad. Sci. U. S. A.*, vol. 113, no. 15, pp. 3932–3937, 2016, doi: 10.1073/pnas.1517384113.

[15] G. R. Bokil, D. Koch, and H. Steeb, “Investigation and Implementation of Machine-Learning-based Hybrid Material Models,” UPC, Escola Tècnica Superior d’Enginyeria de Camins, Canals i Ports de Barcelona, 2022. [Online]. Available: http://hdl.handle.net/2117/387497

[16] J. Bauschinger, “Change of position of the elastic limit under cyclical variations of stress,” *Mitteilungen des Mech. Lab.*, 1881.

[17] J. O. Hallquist and others, “LS-DYNA theory manual,” *Livermore Softw. Technol. Corp.*, vol. 3, pp. 25–31, 2006.